Journal of *Marine Science and Engineering*

MDPI

Article

Effect of Cutting Ratio and Catch on Drag Characteristics and Fluttering Motions of Midwater Trawl Codend

Wei Liu [1], Hao Tang [1,2,3,4,5,*], Xinxing You [6], Shuchuang Dong [7], Liuxiong Xu [1,2,3,4,5] and Fuxiang Hu [6]

1 College of Marine Sciences, Shanghai Ocean University, Shanghai 201306, China; d190200047@st.shou.edu.cn (W.L.); lxxu@shou.edu.cn (L.X.)
2 National Engineering Research Center for Oceanic Fisheries, Shanghai 201306, China
3 Key Laboratory of Oceanic Fisheries Exploration, Ministry of Agriculture and Rural Affairs, Shanghai 201306, China
4 The Key Laboratory of Sustainable Exploitation of Oceanic Fisheries Resources, Shanghai Ocean University, Ministry of Education, Shanghai 201306, China
5 Scientific Observing and Experimental Station of Oceanic Fishery Resources, Ministry of Agriculture and Rural Affairs, Shanghai 201306, China
6 Faculty of Marine Science, Tokyo University of Marine Science and Technology, Minato, Tokyo 108-8477, Japan; yuukinsei@gmail.com (X.Y.); fuxiang@kaiyodai.ac.jp (F.H.)
7 Institute of Industrial Science, The University of Tokyo, 5-1-5 Kashiwanoha, Chiba, Kashiwa 277-8574, Japan; dongsc@iis.u-tokyo.ac.jp
* Correspondence: htang@shou.edu.cn; Tel.: +86-21-61900309

Abstract: The codend of a trawl net is the rearmost and crucial part of the net for selective fish catch and juvenile escape. To ensure efficient and sustainable midwater trawl fisheries, it is essential to better understand the drag characteristics and fluttering motions of a midwater trawl codend. These are generally affected by catch, cutting ratio, mesh size, and twine diameter. In this study, six nylon codend models with different cutting ratios (no cutting, 6:1, 5:1, 4:1, 7:2, and 3:1) were designed and tested in a professional flume tank under two conditions (empty codends and codends with catch) and five current speeds to obtain the drag force, spatial geometry, and movement trend. As the cutting ratio of empty codends decreased, the drag force decreased, and the drag coefficient increased. The unfolding degree of codend netting and the height of empty codends were found to be directly proportional to the current speed and inversely proportional to the cutting ratio. The positional amplitude of codend with cutting ratio 4:1 was the smallest for catch. The drag force of codends with catch increased as the current speed increased, and first decreased and then increased as the cutting ratio decreased. To ensure the best stability and minimum drag force of the codend, it is recommended to use the 4:1 cutting ratio codend.

Keywords: cutting ratio; codend; hydrodynamic characteristics; fluttering motions; the Fourier series

Citation: Liu, W.; Tang, H.; You, X.; Dong, S.; Xu, L.; Hu, F. Effect of Cutting Ratio and Catch on Drag Characteristics and Fluttering Motions of Midwater Trawl Codend. *J. Mar. Sci. Eng.* **2021**, *9*, 256. https://doi.org/10.3390/jmse9030256

Academic Editor: Yuriy Semenov

Received: 24 January 2021
Accepted: 24 February 2021
Published: 28 February 2021

1. Introduction

Trawling plays an important role in marine fishing, accounting for approximately 35% of the world's catches [1,2]. Midwater trawling involves pulling a fishing net horizontally through the water behind one or two vessels. This fishing equipment is normally designed according to the behavior of target species to achieve more selective netting, and to reduce the nets' drag to decrease the fuel consumption of fishing vessels, thus improving fishing efficiency and increasing economic benefits [3,4]. The shape of a midwater trawl is almost similar to an elliptical cone when dragged; the scientific conicity and outline make the midwater trawl smooth and stable, guiding the fish better and with uniform force [5,6]. The conicity and contour of a trawl are obtained by the cutting ratio. However, to ensure that all of the nets of the trawl are at the same inclined angle with a smooth contour, the cutting ratio generally increases from the wing to the codend, causing the trawl

contour line to form a convex curve inwardly when the nets are connected. Then, the curve becomes a straight line by water impact [3].

The codend is connected to the narrow end of a tapered trawl, and is most often an elliptical cone shape due to the cutting ratio [7]. The codend is an essential part of the trawl, because its function is to store large fish by catching them while releasing the juvenile fish [8–10]. However, as the catch accumulates, the codend shape changes, with the front mesh of the codend closing and the rear contour of the codend bulging [11]. To ensure consistent trawl performance, the increase in codend drag as the catch builds up must be considered. Moreover, as the codend is connected to the end of trawl, the effect of shadowing on the codend cannot be ignored [12]. Druault and Germain [13] reported that to optimize the codend efficiency in terms of catchability and its effect on energy consumption, it must have a high static stability, which is difficult due to the significant influence of hydrodynamic turbulence flow. Furthermore, they mentioned that the knowledge of flow instability is important to better understand the force acting on a codend and to implement a selected device.

The selectivity, drag force, and stability of the movement of the codend are significantly affected by the hydrodynamic turbulent boundary layer, vortex, and wake flow developing around the fishing equipment [14]. However, it is difficult to determine the hydrodynamic force on each part of the trawl net because of the fluid–structure interactions that induce large deformation and oscillation of the net, modifying the drag force instantaneously [15,16]. In recent decades, considerable progress has been made in understanding the flow field around a trawl net in general, and a codend in particular, using experimental and numerical approaches. Bouhoubeiny et al. [14] evaluated the flow around rigid and oscillating codend models. These preliminary analyses showed that a symmetrical vortex exists behind the rigid codend and possible turbulent flow interactions with the fluttering codend structure without a complete study of the PIV (Particle Image Velocimetry) database. Recently, Druault and Germain [13] used the PIV method to evaluate the flow field distribution around a codend and found that, while dragging the trawl, vortices are alternately generated behind the codend. The shedding of the vortex generates vertical pressure on the codend and causes it to oscillate. Due to the local hydrodynamic effects (fluctuating velocities, vortex shedding wake, etc.), warp tension variations, movements of the deformable structure itself, and the geometry of rigid structure can cause the codend to oscillate. Moreover, each excitation mechanism can occur simultaneously and interact with each other, thereby increasing the complexity of characterizing the fluid–structure interaction [17]. However, these investigations explain the oscillation of the codend, but do not provide a method to minimize the oscillation amplitude or provide a model to fit the oscillation trend. Madsen et al. [18] evaluated the behavior of six different codends at full scale in a flume tank of SINTEF and found that each codend oscillates considerably when loaded with fish, and the standard codend is the most stable of those six codends. Thus, he considered that adjusting the net type and combination mode of the codend can minimize its oscillation amplitude.

The codend motion and catch build-up in the codend can influence catch quality because they can cause epidermal damage [12,19]. Therefore, it is important to improve the codend performance. As shown by the literature review, there are also differences in the cutting ratio of the codend to suit target species. Kumazawa et al. [20], Zhou et al. [21,22], and Yao et al. [23] investigated the drag characteristics of the midwater trawl, but different cutting ratios of codend structures exist. To date, it has not been determined whether the cutting ratio can be adjusted to reduce the drag force and improve the stability. In addition to influencing the effect of the cutting ratio on attack angle and contour, it also creates a special geometrical shape with the codend that, in turn, influences the hydrodynamic performance of the codend and consequently its catchability, stability, and selectivity. Therefore, in this study, the effects of cutting ratio on the net shape and drag force of empty codends and codends with catch were analyzed. Six codends with different cutting ratios and in two states, with or without catch, were selected. Model tests were performed

under five conditions to compare the net shape, drag force, and motion of these codends. The Fourier series was used to fit the positional and drag force oscillations of the codend with catch, providing information to improve the hydrodynamic performance and stability of the codend.

2. Material and Methods

2.1. Codend Design

The Antarctic krill trawl (codend length = 30 m) is designed for the target vessel, F/V "Long Teng" of China National Fisheries Corp. This net codend has a mesh size of 144 mm and bar diameter of 16 mm. The model trawl codend scales are: length scale = 1/20 (λ = 20), small-scale ratio λ' = 5, flow velocity scale = 1/2.24, according to Tauti's law.

Six models of codends constructed using nylon material and with different cutting ratios were used based on the model codend (Net 1). These codends were constructed by assembling four pieces of netting with a diamond mesh size of 30 mm and a twine diameter of 3 mm. Each piece of netting was joined by part 1 (20 × 25 mesh) and part 2 (20 × 25 mesh), in addition to cutting part 2 into six cutting ratios (no cutting, 6:1, 5:1, 4:1, 7:2, and 3:1). The codend parameters and joining methods are shown in Table 1 and Figure 1.

Table 1. Specifications for each netting panel of codend.

Codend		Twine Materials	Bar Length (mm)	Bar Diameter (mm)	Cutting Ratio	Cutting Sequence (Subscripts Represent Cycle Index)
Part 1		**nylon**	**15**	**3**	**No cutting**	**$[N]_{22}$**
Part 2	**Net 1**	nylon	15	3	No cutting	$[N]_{25}$
	Net 2	nylon	15	3	6:1	N $[NBNNNBN]_4$
	Net 3	nylon	15	3	5:1	$[NBNNBN]_5$
	Net 4	nylon	15	3	4:1	N $[NBNBN]_6$
	Net 5	nylon	15	3	7:2	NB$[NBNBNBNBN]_3$ BNN
	Net 6	nylon	15	3	3:1	$[NBNB]_8$ N

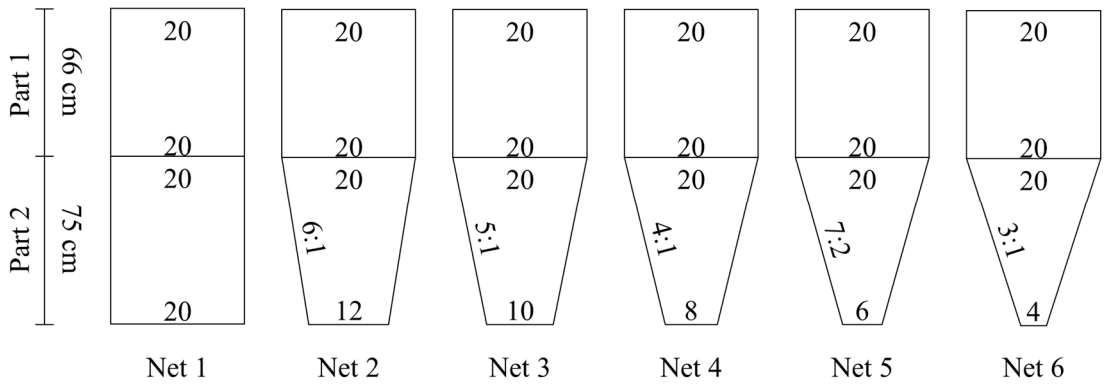

Figure 1. Design sketch of six codends.

2.2. Experimental Setup

Figure 2 shows the experimental apparatus used for measuring the drag force and net shape of the codend. The experiments were conducted in a flume tank at the Tokyo University of Marine Sciences and Technology (TUMST). The test section of the flume tank is 9.0 m in length, 2.2 m in width, and 1.6 m in depth, containing ≈150 tons of freshwater. The flow is circulated using four contrarotating impellers through constant-speed hydraulic delivery pumps. The impellers are 1.6 m in diameter and deliver a maximum flow speed of 2 m/s. A side-viewing window on one side of the flume tank allows users to observe the behavior of the codend during testing and to record video. A camera with a frequency of 59 Hz per frame image and a resolution of 1920 × 1080 pixels was used to record the

codend behavior. To accurately measure the drag force of the codend and ensure that the drag force of the equipment is lower than that of the codend, a circular rigid frame was used to determine the drag force of the codend, and the drag force of the equipment was finally subtracted from the total drag force. In the experiment, the codend opening was joined around the rigid frame, and the rigid frame was combined with a six-component force (5 kgf, Denshikogyo Co., Japan) instrument (Figure 2b). The data were sampled at 50 Hz. A flow meter was placed 1.2 m directly in front of the six-component force instrument to detect the current speed. The measurements were conducted at five different flow velocities of 0.5, 0.6, 0.7, 0.8, and 0.9 m /s. The water density of the flume tank was 999.8 kg/m^3, and the water temperature was maintained at 17.6–18.4 °C during the experiments.

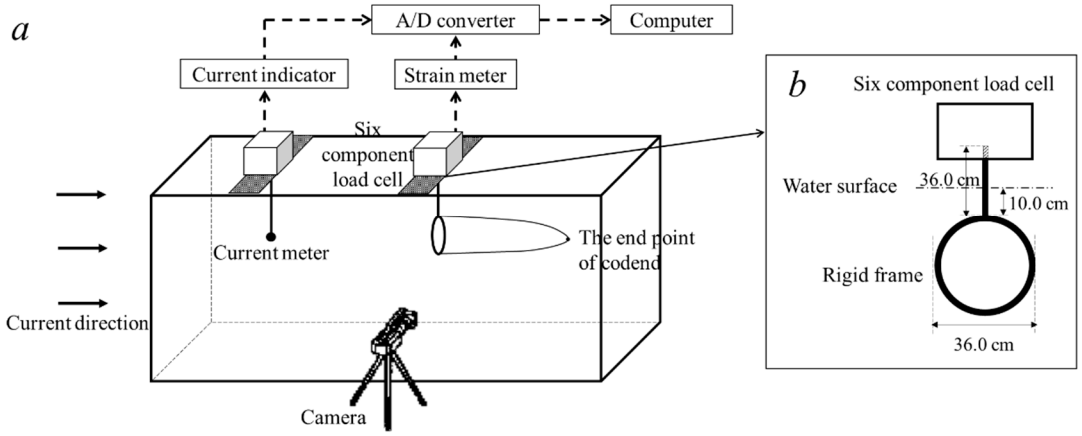

Figure 2. The setup of flume tank experiment (**a**): schematic diagram of experimental set up and apparatus for codend testing; (**b**): schematic diagram of rigid frame).

To measure the drag force and net shape of the codend with catch, a water-injected balloon was used instead of the catch, and a tape measure with an accuracy of 0.1 cm was used to measure the circumference of the balloon at ten different positions. The balloon diameter was calculated as 16.6 ± 0.3 cm, and the density of the water-injected balloon was similar to that of the water in the tank.

2.3. Experimental Procedures

The experiment was divided into two parts with a total of 30 tests. The first part was to measure the drag force and net shape of the empty codend, and the second part was to measure the codend with catch.

Before the experimental measurements of different codends, the drag force of a rigid frame was first measured. The rigid frame was directly combined with the six-component force instrument, making the plane of rigid frame perpendicular to the current direction. This rigid frame handle was immersed in water at 10.0 cm. The drag force of frame was measured at different current velocities, ranging from 0.3 to 1.1 m/s, and set up with an interval of 0.1 m/s. The drag force data measurements of the rigid frame (500 datapoints in total) were sampled for a duration of 10 s, and the average value was calculated using the measurement data.

After the measurement of rigid frame drag force, the second measurement was conducted on the codend without catch. The rigid frame and codend were attached to the six-component instrument and submerged in the water at 10.0 cm, making the rigid frame plane perpendicular to the current direction. The current velocity was adjusted until the codend shape was unfolded and stable. The camera was used directly in front of the observation window to record the net shape of the codend. The drag force and net shape of each codend were recorded for 10 s. Finally, the codend with catch inside (water-injected balloon) was measured, following the same experimental procedure as the first experiment.

The drag coefficient was calculated using Equation (1) as follows:

$$Cx = \frac{2R}{\rho S V^2} \tag{1}$$

where Cx is the drag coefficient, R is the drag force, ρ is the density of water, S is the trawl net opening area, and V is the current speed.

2.4. Data Collection and Analysis

The net shape geometry was obtained from the video camera (Figure 3). The following method was used for image processing in this study: First, a series of images separated by 0.25 s were selected from the recorded video footage; second, graph digitizing software was used to extract the coordinates of characteristic points of the model net based on a plane-coordinate system; finally, a standard bar was used in different locations to calibrate the measurements and consider the effect of camera lens and water refraction. In addition, by maintaining the 50 Hz high-frequency data of drag force for the codend, the high-frequency data were processed to obtain the corresponding 4 Hz data.

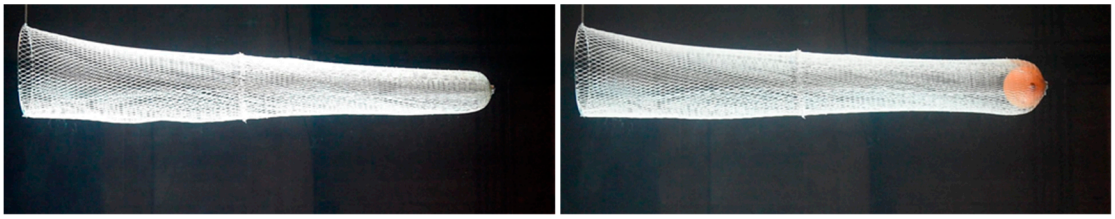

Figure 3. Side-view of the empty codend (**left**) and codend with catch (**right**) in the flume tank.

2.5. Data Fitting and Testing

The Fourier series was used to fit the net motion and drag force oscillation of the codend with catch. The Pearson product-moment correlation coefficient was used to assess the correlation between the fitted and measured values, where 80–100% indicates very strong correlation, 60–80% indicates strong correlation, 40–60% indicates moderate correlation, 20–40% represents weak correlation, and 0–20% indicates very weak correlation or no correlation.

The Fourier series formula can be estimated as follows:

$$f(\mathrm{t}) = \frac{A_0}{2} + \sum_{n=1}^{\infty} (A_n cos\omega_n t + B_n sin\omega_n t) \tag{2}$$

$$\text{or } f(\mathrm{t}) = \frac{A_0}{2} + \sum_{n=1}^{\infty} A_n sin(\omega_n t + \varphi_n) \tag{3}$$

where t is the time, A_n and B_n are amplitude, ω_n is the angular frequency, φ_n is the initial phase, and n is the series.

The Pearson product-moment correlation coefficient can be calculated using Equation (4):

$$\rho_{XY} = \frac{Cov(X,Y)}{\sqrt{D(X)}\sqrt{D(Y)}} = \frac{E\{[X - E(X)][Y - E(Y)]\}}{\sqrt{D(X)}\sqrt{D(Y)}} \tag{4}$$

where E is the mean, D is the variance, $\sqrt{D(X)}$ and $\sqrt{D(Y)}$ are the standard deviation of variables X and Y, and $E\{[X - E(X)]\,[Y - E(Y)]\}$ is the covariance of variables X and Y, denoted $Cov(X, Y)$, i.e., $Cov(X, Y) = E\{[X - E(X)]\,[Y - E(Y)]\}$.

3. Results

3.1. Frame Drag Force

To verify the effectiveness of the experimental frame, the rigid frame drags were measured at different current speeds (Figure 4). The rigid frame drag force varied from 32.5 to 541.4 g as the current speed varied from 0.3 to 1.1 m/s. The results indicate that the rigid frame drag increased as the current speed increased, and their relationship was exponential (Figure 4). Using nonlinear regression with the data argument predicted from the formula of drag force of rigid frame with different current speeds, the following expression is proposed:

$$R_{frame} = 422.47 \times {V_{flow}}^{2.070}, \left(R^2 = 0.99\right) \quad (5)$$

where R_{frame} is the drag force of the rigid frame and V_{flow} is the current speed.

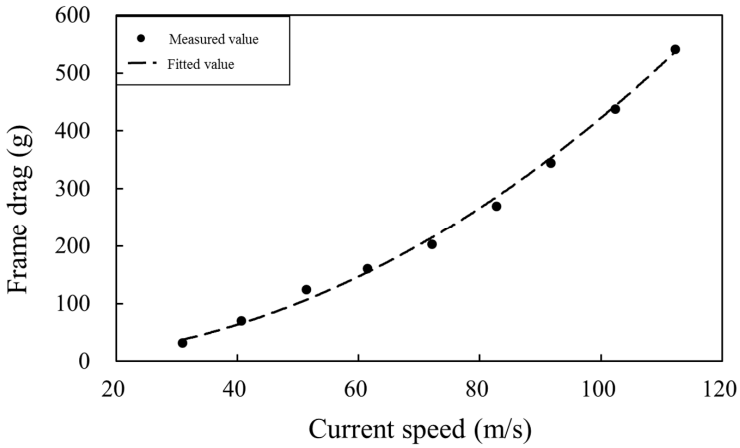

Figure 4. The relationship between frame drag and current speed.

3.2. Empty Codend Profile

As shown in Figure 5, the codend motion increases as the current speed increases. The codend without cutting droops the most at a current speed ≤0.6 m/s. However, at a current speed of ≥0.8 m/s, the central axis of each codend is horizontal. Moreover, the unfolding degree of codend netting and the height of the codend endpoint are directly proportional to the current speed and inversely proportional to the cutting ratio.

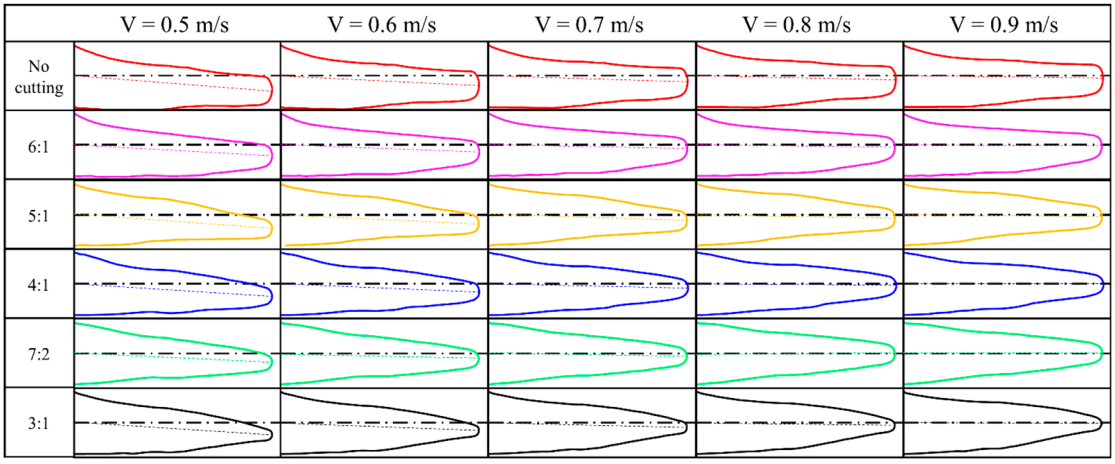

Figure 5. Variation of the profile of empty codends with different cutting ratios at different current speeds.

3.3. Drag Force of Empty Codends

The drag forces on the codends were determined by subtracting the averaged measurements for each current speed on the rigid frame from the averaged measurements for each current speed on the frame and codends; the results are shown in Figure 6. The codends' drag force increased as the current speed and cutting ratio increased. On average, the drag forces of codend without cutting are 9.44% (±0.94%), 13.25% (±0.67%), 16.68% (±0.81%), 16.05% (±1.04%), and 18.24% (±0.95%) greater than those of codend with cutting ratios 6:1, 5:1, 4:1, 7:2, and 3:1, respectively.

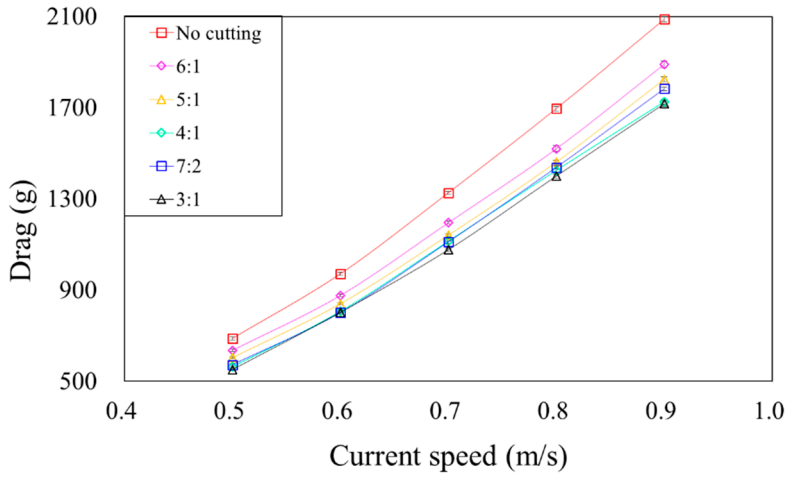

Figure 6. Drag of empty codends with different cutting ratio at 5 current speeds.

On average, the drag coefficients of codend without cutting are 2.99% (±0.66%), 3.04% (±0.53%), 3.09% (±1.44%), 7.72% (±0.32%), and 9.33% (±1.19%) smaller than those of codend with cutting ratios 6:1, 5:1, 4:1, 7:2, and 3:1, respectively (Figure 7). The drag coefficient of the codend decreased as the Reynolds number and cutting ratio increased (Figure 7). Moreover, the codends with cutting ratios 6:1, 5:1, 4:1, 7:2, and 3:1 were designed to have a small amount of twine compared with codends without cutting and those used in the midwater fishing industry to evaluate the effect of cutting ratio on the total drag.

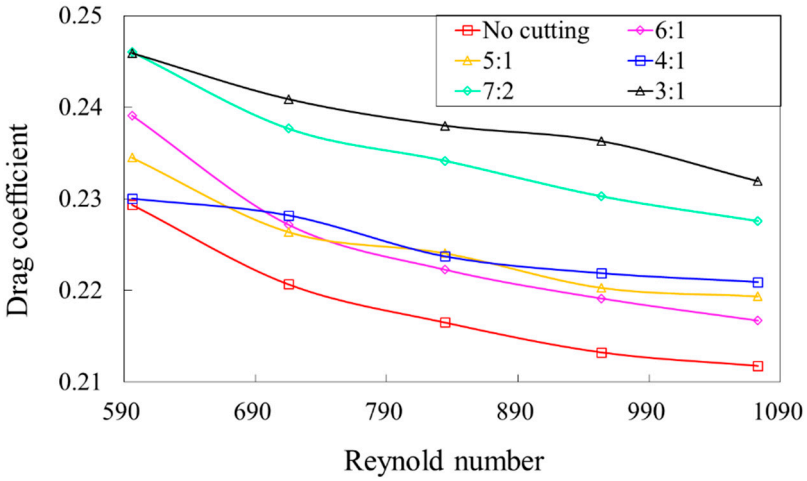

Figure 7. Drag coefficient of empty codends with different cutting ratio at five current speeds.

3.4. Positional Oscillation of Codends with Catch

Evaluation of fluid–structure–catch interaction requires consideration of the geometry and motions of codend structure. Figure 8 shows the time evolution of fluctuating transverse motion of codend structure with catch inside during selected measurements. Clearly, the codend oscillates when it has a catch. However, using the first-order and second-order

Fourier series to fit the positional oscillation, the results show that as the current speed increased, the oscillation cycle of each codend decreased, but the amplitude did not change significantly with a gap of <1.5%. Except for the amplitude of codend without the cutting ratio, the amplitude first decreased (current speed lower than 0.7 m/s) and then increased (current speed higher than 0.7 m/s) as the cutting ratio decreased.

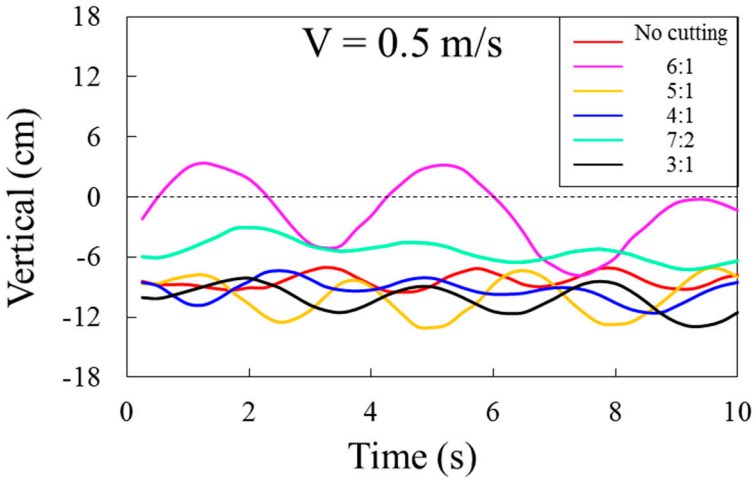

Figure 8. Variations of the end point height for codends with catch in different cutting ratios.

3.5. Use of Fourier Series to Fit the Positional Oscillation of Codends

The Fourier series was used to fit the positional oscillation of the codend, and the Pearson product-moment correlation coefficient was used to test the fitted value (Figure 9, Table 2). The results show that when the first-order Fourier series was used to fit the motion of codend, the fitted value was the same as the measured value with a very strong correlation (43.3%), but others still have an error compared with the measured value because of a moderate correlation of 10%. When the second-order Fourier series was used, the fitted value showed a very strong correlation of 93.3% compared with the measured value, and the remaining (6.7%) had a strong correlation.

Table 2. Correlation of measured value and fitted value of the end point height for codends by the Pearson product-moment correlation coefficient.

		Cutting Ratio						
First-order Fourier Series		**No Cutting**	**6:1**	**5:1**	**4:1**	**7:2**	**3:1**	**Average**
Current speed (m/s)	0.5	79.0%	88.3%	91.9%	71.8%	66.9%	85.2%	80.5%
	0.6	94.5%	91.0%	80.4%	70.6%	75.8%	91.8%	84.0%
	0.7	92.5%	86.6%	96.1%	56.2%	77.8%	86.8%	82.7%
	0.8	92.2%	74.6%	68.0%	70.1%	58.3%	89.9%	75.5%
	0.9	77.8%	62.5%	79.1%	76.0%	53.2%	84.1%	72.1%
Second-order Fourier Series								
Current speed (m/s)	0.5	88.8%	90.5%	94.0%	95.4%	97.4%	92.0%	93.0%
	0.6	96.4%	96.3%	89.3%	89.9%	98.1%	92.2%	93.7%
	0.7	93.0%	96.5%	98.0%	87.3%	94.6%	96.7%	94.3%
	0.8	94.8%	95.5%	78.5%	75.6%	85.6%	93.7%	87.3%
	0.9	90.7%	84.9%	86.7%	84.4%	83.4%	89.1%	86.5%

Note: Percentage values represent the similarity between the Fourier series fitted value and the measured value.

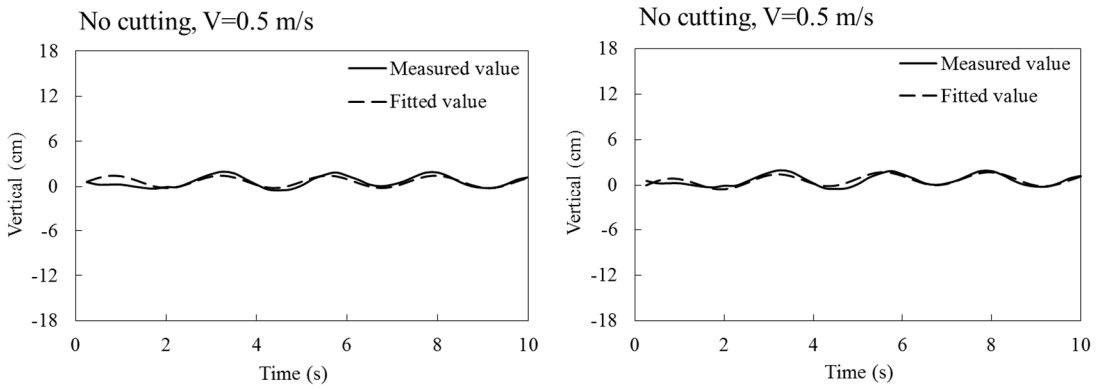

Figure 9. Comparison of the fitted value and the measured value of the end point height for codends with catch using different order Fourier series (an example: (**left**): using the first-order Fourier series; (**right**): using the second-order Fourier series).

3.6. Drag Force of Codends with Catch

The drag force of codends with catch increased as the current speed increased; however, when the cutting ratio decreased, the drag force first decreased and then increased, except the drag force of the 4:1 cutting ratio, which was lower than those of other codends (Figure 10). Furthermore, as shown in Figure 10, the drag force evolution of codends was quasi-periodic oscillatory. The oscillations include high-frequency (50 Hz) and low-frequency (4 Hz). However, no significant difference was observed between the high-frequency and low-frequency oscillation of each codend in the first-order Fourier series. In contrast, when the second-order and third-order Fourier series were used to fit the low-frequency oscillation, the amplitude of each codend drag force increased, and the cycle decreased with the increase in current speed. Moreover, the oscillation cycle of each codend drag force had no significant difference in terms of cutting ratio at the same current speed, but the amplitude initially decreased and then increased as the cutting ratio decreased. The amplitude of codend without the cutting ratio is the highest, and that of 4:1 cutting ratio codend is the smallest, compared to those of other codends.

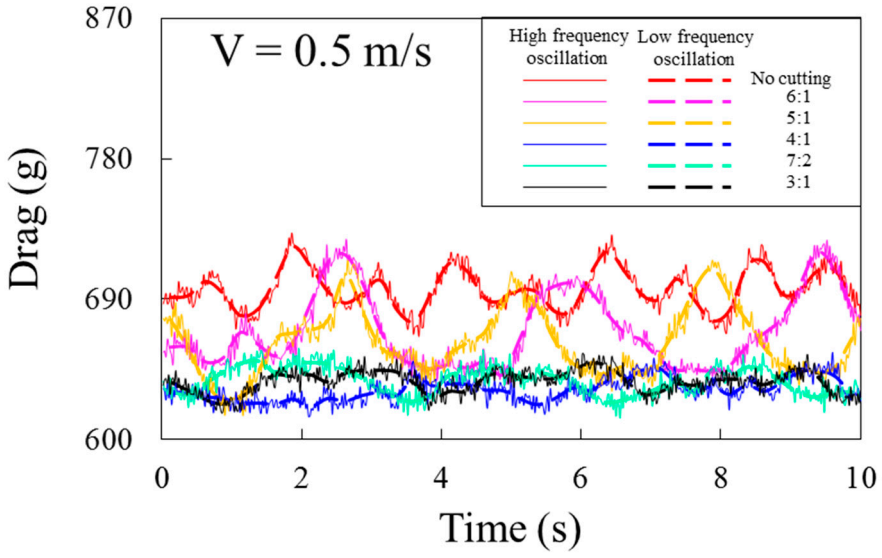

Figure 10. Variations of drag for codends with catch in different cutting ratios.

3.7. Use of Fourier Series to Fit the Drag Force Oscillation of Codends

The Fourier series can be used to fit the drag force oscillation of a codend. However, the accuracy of the fitted value obtained using the second-order Fourier series is different from that obtained using the third-order Fourier series (Figure 11). Using the Pearson

product-moment correlation coefficient to test the fitted and measured values (Table 3), the use of second-order Fourier series to fit the measured value has a lower correlation with very strong correlation (56.7%), but the use of third-order Fourier series to fit the drag force of codend with different cutting ratios has also very strong correlation with the increase in measured value to 86.7%.

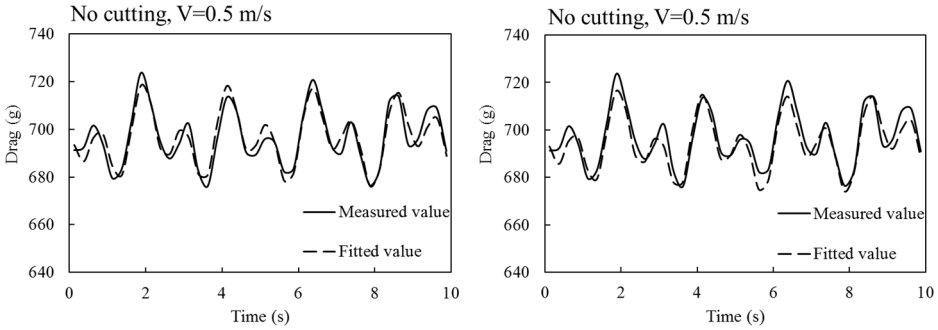

Figure 11. Comparison of the fitted value and the measured value of drag for codends with catch using different order Fourier series (an example: (**left**): using the second-order Fourier series; (**right**): using the third-order Fourier series).

Table 3. Correlation of measured value and fitted value of codend drag by the Pearson product-moment correlation coefficient.

		Cutting Ratio						
Second-order Fourier Series		**No Cutting**	**6:1**	**5:1**	**4:1**	**7:2**	**3:1**	**Average**
Current speed (m/s)	0.5	94.0%	95.1%	92.9%	81.7%	88.0%	87.8%	89.9%
	0.6	91.3%	81.4%	89.6%	69.9%	69.4%	66.0%	77.9%
	0.7	76.7%	72.8%	92.3%	73.7%	87.5%	50.3%	75.5%
	0.8	82.7%	76.7%	70.2%	72.6%	93.5%	81.0%	79.4%
	0.9	81.5%	70.3%	76.9%	63.9%	85.3%	94.4%	78.7%
Third-order Fourier Series								
Current speed (m/s)	0.5	94.5%	97.4%	95.6%	84.5%	89.8%	92.3%	92.3%
	0.6	92.2%	86.0%	90.9%	80.7%	90.9%	82.5%	87.2%
	0.7	85.9%	81.4%	94.0%	83.4%	93.5%	73.3%	85.3%
	0.8	85.0%	84.6%	72.2%	82.0%	94.4%	88.2%	84.4%
	0.9	86.3%	79.0%	85.2%	74.6%	90.7%	96.7%	85.4%

Note: Percentage values represent the similarity between the Fourier series fitted value and the measured value.

4. Discussion

4.1. Effect of Rigid Frame Drag Force on Codend

The experimental apparatus effect of model nets is a common problem, especially in codend model tests. This study and previous studies by Pichot et al. [24], Bouhoubeiny et al. [14], and Druault and Germain [13] used a self-designed configuration of this rigid frame to accurately measure the hydrodynamic forces of the codend. One of the principal objectives in fishing gear hydrodynamic measurements is to design frames with very lower drag forces unlike those of fishing equipment in general, and nettings or codends in particular. In this case, the average drag force caused by a rigid frame was 17.6% (±1.3%) and 16.1% (±0.7%) of the total compared to the codend without catch and with catch (codend drag + rigid frame drag), respectively. In addition, the frame stability was evaluated under different current speeds and cutting ratios. Indeed, the ratio between drag force caused by a rigid frame without a codend and the total drag increased as current speed and cutting ratio increased. This ratio was 13.32% (±0.42%), 14.51% (±0.54%), 15.05% (±0.49%), 15.60% (±0.46%), 15.47% (±0.35%), and 15.82% (±0.40%) for the codend without cutting ratio and the codends with cutting ratios 6:1, 5:1, 4:1, 7:2, and 3:1, respectively. However, the results reported by Tang et al. [25,26] on netting showed that the frame drag force

accounted for a maximum of between 17% and 20% of the total (netting drag + rigid frame drag) using streamlined frames, close to those obtained in this experiment. Therefore, the application of a rigid frame reduced the impact of turbulent or vortex flow on the experimental hydrodynamic force and the geometrical shape of codends. When studying hydrodynamic forces and codend motion at different current speeds, the use of a rigid frames is strongly recommended.

4.2. Effect of Cutting Ratio on the Net Shape and Drag Force of Empty Codends

In this study, the codend did not oscillate significantly under the condition of an empty codend. Unlike the results of previous studies, the results obtained by Pichot [27] and Bouhoubeiny et al. [14] using a rigid codend showed that an asymmetrical vortex was generated at the codend tail due to the obstruction of codend. At the same time, the vortex shedding generated water pressure in the vertical flow direction to the codend and caused an oscillation of this structure. The differences between the results obtained in this study and those obtained by Bouhoubeiny et al. [14] are due to the codend filtration and the current speed, which are not the same. In addition, the difference is also because Bouhoubeiny et al. [14] placed a spherical cap to block the water directly passing through the mesh of the codend at the codend bottom, but allowed the water to flow back and around the outer surface of the spherical cap, thereby generating a symmetrical vortex. In this study, the codend was completely open, facilitating the passage of water through the mesh of the codend and not causing a vortex in the codend that would deviate the fish trajectory. Indeed, the bar of mesh also blocks the water passing through the codend directly [24,28,29], but the pressure generated by the shading effect of the bar was not sufficient to make the entire codend oscillate significantly. Thus, the codend did not significantly oscillate in the camera shot.

As shown in the side view of each codend shape in Figure 5, the lower part of the codend without cutting ratio had obvious stacking at a low current speed, and the stacking nets rippled with the current in the video. These results were also observed in the study carried out by Balash and Sterling [30] on prawn trawl, Bouhoubeiny et al. [31] on the flow measurement around a fishing net, and Tang et al. [32] on the shape measurement of a purse seine. However, according to the drag force results obtained in each empty codend at different current speeds (Figure 6), the drag force of the empty codend positively correlates with the cutting ratio, i.e., a higher cutting ratio led to a greater drag force of codend at the same current speed. Thus, the reason is not only that the cutting ratio was directly proportional to the twine area, but also that the codend with a high cutting ratio was more likely to stack the net under the low current speed condition, thus increasing its drag force. A significant decrease in twine area and drag force was observed due to a decrease in cutting ratio. Indeed, the twine area of the codend without a cutting ratio was 7.81%, 9.96%, 12.20%, 14.52%, and 16.96% greater than that of codends with cutting ratios of 6:1, 5:1, 4:1, 7:2, and 3:1, respectively. As mentioned above, the codends with cutting ratio were designed to contain a small amount of twine compared to codends without a cutting ratio and those used in the midwater trawl fishery industry to demonstrate the effect of the cutting ratio on hydrodynamic force and net shape. In conclusion, according to the experimental results of Balash et al. [33] and Thierry et al. [3] on the effect of net cutting of the prawn trawl body and bottom trawl wing on the trawl performance, and the results of this study, the net cutting of some part of the trawl net allows it to change its shape, which automatically reduces its twine area and drag force while making it more efficient.

This study also demonstrated that the increase in cutting ratio led to the increase in the angle between the flow direction and codend surface (attack angle) during the operation. However, Tang et al. [25] reported that the relationship between the nylon mesh drag coefficient and attack angle (0°–20°) has a positive correlation, and the netting drag coefficient increased as the attack angle increased, decreasing as the Reynolds number increased before moving asymptotically toward a constant value. This trend was confirmed by the experiment carried out in this study, demonstrating that the drag coefficient for the

empty codend increased as the Reynolds number decreased and attack angle and cutting ratio increased. However, the drag coefficients obtained in this study are different from those obtained in the netting by Tang et al. [25,26,34] and Hosseini et al. [35], whereas they are similar to those obtained on the optimized trawls studied by Balash [30] and Thierry et al. [6]. The main reason for this difference is that the mesh of the codend is in a free state in this experiment, rather than the mesh being tightly bound to the frame. In addition, the net at the bottom of the codend piles up and waves with the current. Moreover, the attack angles are not the same in the whole codend structure, and the shadowing effect of the rigid frame affected the codend drag coefficient. By comparing the effect of the cutting ratio and twine area on the codend drag force, it can be seen that the effect of twine area on the drag force for the codend is greater.

4.3. Effect of Catch Substitutes on the Experiment

The actual catch build-up in a codend produces debris and fall, affecting the outcome and equipment. Some researchers use catch substitutes for model experiments. The catch substitutes are generally divided into two categories, namely multiple small-volume objects and a single large-volume object. The multiple small-volume objects mainly include water-filled table tennis balls or small-volume water-filled bags. Madsen et al. [18] used multiple small-volume water-filled bags to evaluate the effects of mesh types on the hydrodynamics and oscillations of the codend. Multiple small objects in the codend directly block the flow through the mesh, similar to the actual catch when investigating the flow field distribution. However, because small objects have a smooth surface and most of them are spherical with a large space, the overall drag force of the model is less than the actual drag force. In addition, the number of small-volume objects required in the test is mostly large; operating errors can cause some small-volume objects to pass into the tank and damage the instrument. Single large-volume objects mainly include a water-injected balloon or a spherical cap. When Druault and Germain [13] used the PIV technology to study the effect of catch on shadowing and flow field around the codend, a spherical cap and water-injected balloon were used in the place of catches. Such a surrogate also plays a role in blocking the flow directly through the mesh, but it completely blocks the flow. Therefore, the use of a single large volume to replace the catch will result in an overall drag force of the codend that is greater than that actually obtained, and also makes the oscillation of codend more obvious. The drag focus in this study was to analyze the effect of the cutting ratio on the oscillation of the codend. Obvious codend oscillation allowed easy result analysis, so a water-injected balloon was used instead of real catch.

4.4. Effect of Cutting Ratio on the Shape and Drag Force Oscillation of Codends with Catch

A codend with catch has obvious oscillations in position or drag force. Previously, Bouhoubeiny et al. [14], Madsen et al. [18], and Druault and Germain [13] reported that codend oscillations can be caused by the vortices behind the codend. When dragging the trawl, vortex shedding generates vertical pressure on the codend and makes it oscillate. Furthermore, this study and Madsen et al. [18] found that codend oscillation is not limited to the specific direction, but codend oscillation in any direction perpendicular to the codend central axis is possible. The main reason is that the codend motion is free in all directions perpendicular to the central axis. In addition, the oscillating track of the codend is mainly distributed near the central axis according to the results obtained by this experiment and Madsen et al. [18].

The codend drag force oscillation mainly included a high-frequency oscillation and a low-frequency oscillation according to the results obtained in this study and those obtained by Bouhoubeiny et al. [14] and Druault and Germain [13]. In addition, it was also found that the low-frequency oscillation of codend drag force included strong wave oscillation (large amplitude) and weak wave oscillation (small amplitude), and the strong wave and weak wave oscillations appeared alternately. The sum of two oscillating cycles of drag force is approximately equal to one oscillating cycle of the position. Moreover, this experiment

and those of Bouhoubeiny et al. [14] and Druault and Germain [13] also confirmed that the oscillation of codend position and drag force oscillation are synchronous, i.e., the alternate cycle of two vortices in the same direction is equal to one codend positional oscillation cycle.

Because of two main factors, namely, the twine area and attack angle, the positional and drag force oscillation amplitudes of large cutting ratios (no cutting, 6:1, and 5:1) are usually greater than those of small cutting ratios (4:1, 7:2, and 3:1). A larger cutting ratio can lead to a larger twine area, making the codend drag force greater. Therefore, the vortex shedding generates more vertical pressure on the codend and increases the amplitude. The periodic variation in the oscillation is mainly due to the periodicity of vortex shedding [13]. The greater the current speed, the greater the vortex shedding speed, and the greater the pressure. This also shows that, as the current speed increases, the oscillation cycle is shorter and leads to a greater amplitude. In addition, according to the orthogonal decomposition analysis, the amplitude decreased as the attack angle and binding force of free direction (vertical current direction) increased.

4.5. Fourier Series Fitting

The Fourier series was used in this study to fit cyclic motion. The higher the series, the closer the fitted value to the measured value, but the calculation increased as the series increased. In this study, the first-order and second-order Fourier series were used to fit the codend positional oscillation. The results show that the value obtained using the second-order Fourier series is close to the measured value, depending on the positional oscillation of the codends with catch taken in a different cutting ratio (Figure 8). This also shows that the codend positional oscillation has a trigonometric function, with the exception of the presence of alternate strong and weak waves of positional oscillation, such as a 6:1 cutting ratio with 0.8 and 0.9 m/s. Therefore, when fitting the codend positional oscillation, it is recommended to use $\geq$ second-order Fourier series to fit the codend positional oscillation.

The Fourier series was used to fit the oscillation of codend drag force which should be greater than that of positional oscillation fitting. As shown in Figure 10, the force oscillation of the codend included high-frequency oscillation and low-frequency oscillations. The low-frequency oscillations included strong wave oscillation and weak wave oscillation. In this study, we only fitted low-frequency oscillation. The results show that although a third-order Fourier series was used to fit the codend drag force oscillations, some of the fitted values were still different from the measured values. Therefore, when using the Fourier series to fit the low-frequency oscillation of the codend drag force, it is recommended to use $\geq$ third-order Fourier series.

Author Contributions: Literature, W.L. and S.D.; figures, W.L. and S.D.; study design, W.L., H.T., X.Y., L.X., and F.H.; data collection, W.L., H.T., X.Y., L.X. and F.H., funding acquisition, H.T. and L.X.; data analysis, W.L. H.T., S.D. and F.H.; writing—original draft, W.L.; writing—review and editing, W.L. and H.T. All authors have read and agreed to the published version of the manuscript.

Funding: This study was financially sponsored by the National Natural Science Foundation of China (Grand No. 31902426), Shanghai Sailing Program (19YF1419800), and Special project for the exploitation and utilization of Antarctic biological resources of Ministry of Agriculture and Rural Affairs (D-8002-18-0097).

Institutional Review Board Statement: Not applicable.

Informed Consent Statement: Not applicable.

Data Availability Statement: Not applicable.

Conflicts of Interest: The authors declare no conflict of interest.

References

1. Watson, R.; Revenga, C.; Kura, Y. Fishing gear associated with global marine catches: II. Trends in trawling and dredging. *Fish. Res.* **2006**, *79*, 103–111. [CrossRef]
2. Anticamara, J.A.; Gelchu, R.; Watson, A.; Pauly, D. Global fishing effort (1950–2010): trends, gaps, and implications. *Fish. Res.* **2011**, *107*, 131–136. [CrossRef]
3. Thierry, N.N.B.; Tang, H.; Achile, N.P.; Xu, L.; Hu, F.; You, X. Comparative study on the full-scale prediction performance of four trawl nets used in the coastal bottom trawl fishery by flume tank experimental investigation. *Appl. Ocean Res.* **2020**, *95*, 102022. [CrossRef]
4. Sala, A.; De Carlo, F.; Buglioni, G.; Lucchetti, A. Energy performance evaluation of fishing vessels by fuel mass flow measuring system. *Ocean Eng.* **2011**, *38*, 804–809. [CrossRef]
5. Park, H.-H.; Cho, B.-K.; Ko, G.-S.; Chang, H.-Y. The gear shape and cross section of sweep at mouth of a bottom trawl. *J. Korean Soc. Fish. Technol.* **2008**, *44*, 120–128. [CrossRef]
6. Thierry, N.N.B.; Tang, H.; Liuxiong, X.; You, X.; Hu, F.; Achile, N.P.; Kindong, R. Hydrodynamic performance of bottom trawls with different materials, mesh sizes, and twine thicknesses. *Fish. Res.* **2020**, *221*, 105403. [CrossRef]
7. Wileman, D.A.; Ferro, R.S.T.; Fonteyne, R.; Millar, R.B. (Eds.) *Manual of Methods of Measuring the Selectivity of Towed Fishing Gears*; ICES Cooperative Research Report No. 215; International Council for the Exploration of the Sea (ICES): Copenhagen, Denmark, 1996; Available online: http://www.vliz.be/imisdocs/publications/266109.pdf (accessed on 27 February 2021).
8. Brčić, J.; Herrmann, B.; Sala, A. Predictive models for codend size selectivity for four commercially important species in the Mediterranean bottom trawl fishery in spring and summer: Effects of codend type and catch size. *PLoS ONE* **2018**, *13*, e0206044. [CrossRef] [PubMed]
9. Sala, A.; Herrmann, B.; De Carlo, F.; Lucchetti, A.; Brčić, J. Effect of codend circumference on the size selection of square-mesh codends in trawl fisheries. *PLoS ONE* **2016**, *11*, e0160354. [CrossRef]
10. Sala, A.; Lucchetti, A.; Buglioni, G. The influence of twine thickness on the size selectivity of polyamide codends in a Mediterranean bottom trawl. *Fish. Res.* **2007**, *83*, 192–203. [CrossRef]
11. O'Neill, F.G.; O'Donoghue, T. The fluid dynamic loading on catch and the geometry of trawl cod–ends. *Proc. R. Soc. A Math. Phys. Eng. Sci.* **1997**, *453*, 1631–1648. [CrossRef]
12. O'Neill, F.; Knudsen, L.; Wileman, D.; McKay, S. Cod-end drag as a function of catch size and towing speed. *Fish. Res.* **2005**, *72*, 163–171. [CrossRef]
13. Druault, P.; Germain, G. Analysis of hydrodynamics of a moving trawl codend and its fluttering motions in flume tank. *Eur. J. Mech. B Fluids* **2016**, *60*, 219–229. [CrossRef]
14. Bouhoubeiny, E.; Germain, G.; Druault, P. Time-resolved PIV investigations of the flow field around rigid cod-end net structure. *Fish. Res.* **2011**, *108*, 344–355. [CrossRef]
15. Liu, L.; Kinoshita, T.; Wan, R.; Bao, W.; Itakura, H. Experimental investigation and analysis of hydrodynamic characteristics of a net panel oscillating in water. *Ocean Eng.* **2012**, *47*, 19–29. [CrossRef]
16. Zheng, Z.; Zhang, N. Frequency effects on lift and drag for flow past an oscillating cylinder. *J. Fluids Struct.* **2008**, *24*, 382–399. [CrossRef]
17. Blevins, R.D.; Saunders, H. Flow Induced Vibration. *J. Mech. Des.* **1979**, *101*, 6. [CrossRef]
18. Madsen, N.; Hansen, K.; Madsen, N.A.H. Behavior of different trawl codend concepts. *Ocean Eng.* **2015**, *108*, 571–577. [CrossRef]
19. Wan, R.; Jia, M.; Guan, Q.; Huang, L.; Cheng, H.; Zhao, F.; He, P.; Hu, F. Hydrodynamic performance of a newly-designed Antarctic krill trawl using numerical simulation and physical modeling methods. *Ocean Eng.* **2019**, *179*, 173–179. [CrossRef]
20. Kumazawa, T.; Hu, F.X.; Watanabe, T.; Kinoshita, H.; Tokai, T. Development of a Pelagic and/or Mid Water Trawl with Canvas Kites. *Fish. Eng.* **2010**, *46*, 197–204. Available online: http://ci.nii.ac.jp/naid/110007580742 (accessed on 27 February 2021).
21. Zhou, A.Z.; Zhang, Y.; Wang, Y.J.; Zhang, X. Comparison on the Hydrodynamic Performance of Mid-Water Trawl 1056 Type for Catching Small Upper-Middle-Class Fish in Middle-East Atlantic and 1040 Type Mid-Water Trawl for Catching Chilean Jack Mackerel. *Fish. Inf. Strategy* **2015**, *2*, 112–118. Available online: http://en.cnki.com.cn/Article_en/CJFDTOTAL-XYYZ201502006.htm (accessed on 27 February 2021).
22. Zhou, A.Z.; Feng, C.L.; Zhang, X.; Wang, Y.J. Influence of Adjustment of Operation Parameters on Small-Mesh Antarctic Krill trawl. *Mar. Fish.* **2016**, *1*, 74–82. Available online: http://www.en.cnki.com.cn/Article_en/CJFDTotal-HTYY201601010.htm (accessed on 27 February 2021).
23. Yao, Y.; Chen, Y.; Zhou, H.; Yang, H. A method for improving the simulation efficiency of trawl based on simulation stability criterion. *Ocean Eng.* **2016**, *117*, 63–77. [CrossRef]
24. Pichot, G.; Germain, G.; Priour, D. On the experimental study of the flow around a fishing net. *Eur. J. Mech. B Fluids* **2009**, *28*, 103–116. [CrossRef]
25. Tang, H.; Xu, L.X.; Hu, F.X. Hydrodynamic characteristics of knotted and knotless purse seine net panels as determined in a fume tank. *PLoS ONE* **2018**, *13*, e0192206. [CrossRef] [PubMed]
26. Tang, H.; Hu, F.; Xu, L.; Dong, S.; Zhou, C.; Wang, X. Variations in hydrodynamic characteristics of netting panels with various twine materials, knot types, and weave patterns at small attack angles. *Sci. Rep.* **2019**, *9*, 1–13. [CrossRef]

27. Pichot, G. Modélisation et Analyse Numérique du Couplage Filet-Écoulement Hydrodynamique dans une Poche de Chalut. Ph.D. Thesis, Université de Rennes, Rennes, France, 6 December 2007. Available online: https://archimer.ifremer.fr/doc/2007/these-3350.pdf (accessed on 27 February 2021).
28. Bi, C.-W.; Balash, C.; Matsubara, S.; Zhao, Y.-P.; Dong, G.-H. Effects of cylindrical cruciform patterns on fluid flow and drag as determined by CFD models. *Ocean Eng.* **2017**, *135*, 28–38. [CrossRef]
29. Bearman, P. Vortex shedding from oscillating bluff bodies. *Annu. Rev. Fluid Mech.* **1984**, *16*, 195–222. [CrossRef]
30. Balash, C.; Sterling, D. Prawn trawl drag due to material properties-an investigation of the potential for drag reduction. *J. Appl. Phys.* **2012**, *46*, 1376–1381. [CrossRef]
31. Bouhoubeiny, E.; Druault, P.; Germain, G. Phase-averaged mean properties of turbulent flow developing around a fluttering sheet of net. *Ocean Eng.* **2014**, *82*, 160–168. [CrossRef]
32. Tang, H.; Xu, L.; Hu, F.; Kumazawa, T.; Hirayama, M.; Zhou, C.; Wang, X.; Liu, W. Effect of mesh size modifications on the sinking performance, geometry and forces acting on model purse seine nets. *Fish. Res.* **2019**, *211*, 158–168. [CrossRef]
33. Balash, C.; David, S.; Jonathan, B.; Giles, T.; Neil, B. Drag characterisation of prawn-trawl bodies. *Ocean Eng.* **2016**, *113*, 18–23. [CrossRef]
34. Tang, H.; Hu, F.; Xu, L.; Dong, S.; Zhou, C.; Wang, X. The effect of netting solidity ratio and inclined angle on the hydrodynamic characteristics of knotless polyethylene netting. *J. Ocean Univ. China* **2017**, *16*, 814–822. [CrossRef]
35. Hosseini, S.A.; Lee, C.-W.; Kim, H.-S.; Lee, J.; Lee, G.-H. The sinking performance of the tuna purse seine gear with large-meshed panels using numerical method. *Fish. Sci.* **2011**, *77*, 503–520. [CrossRef]